



Kinetic Isotope Effect Analysis of RNA 2'-O-Transphosphorylation

Michael E. Harris^{*,1}, Darrin M. York[†], Joseph A. Piccirilli[‡],
Vernon E. Anderson[§]

^{*}University of Florida, Gainesville, FL, United States

[†]Rutgers University, Piscataway, NJ, United States

[‡]The University of Chicago, Chicago, IL, United States

[§]Case Western Reserve University School of Medicine, Cleveland, OH, United States

¹Corresponding author: e-mail address: harris@chem.ufl.edu

Contents

1. Introduction	434
1.1 Mechanisms and Transition States of RNA 2'-O-Transphosphorylation Reactions	435
1.2 Application of KIE Analyses to Investigate Transition States of RNA Strand Cleavage Reactions	438
2. Synthesis of Isotopomer RNA Substrates Enriched in ¹⁸ O at the Reacting Phosphoryl Oxygens	439
2.1 [2'- ¹⁸ O]Uridine	439
2.2 [5'- ¹⁸ O]Guanosine	440
2.3 [¹⁸ O] Incorporation Into NPOs	441
3. Use of Electrospray Ionization Quadrupole/Time-of-Flight Mass Spectrometry to Measure ¹⁸ O KIEs for RNA 2'-O-transphosphorylation	441
3.1 Determination of Reaction Kinetics and Purification of Substrates and Products Using HPLC	441
3.2 Determination of ¹⁶ O/ ¹⁸ O Ratios in 5'-UpG-3' by Tandem Q/TOF MS	445
3.3 Data Fitting and Calculation of KIEs Using Internal Competition Kinetics	450
4. Future Directions	453
References	454

Abstract

The breaking of RNA strands by 2'-O-transphosphorylation is a ubiquitous reaction in biology, and enzymes that catalyze this reaction play key roles in RNA metabolism. The mechanisms of 2'-O-transphosphorylation in solution are relatively well studied, but complex and can involve different transition states depending on how the reaction is catalyzed. Because of this complexity and the lack of experimental information on transition-state structure, pinning down the chemical details of enzyme-catalyzed RNA strand cleavage has been difficult. Kinetic isotope effects (KIEs) provide information about changes in bonding as a reaction proceeds from ground state to transition state,

and therefore they provide a powerful tool for revealing mechanistic detail. Application of kinetic isotope analyses to RNA 2'-*O*-transphosphorylation faces three fundamental challenges: synthesis of RNA substrate isotopomers with ^{18}O substitutions at the 2'-*O*, 5'-*O* and nonbridging phosphoryl oxygens; determination of the $^{18}\text{O}/^{16}\text{O}$ ratios in the residual unreacted substrate or product RNAs; and analyzing these data to allow calculation of the KIEs for use in evaluating different mechanistic scenarios. In this chapter, we outline methods for surmounting these challenges for solution RNA 2'-*O*-transphosphorylation reactions, and we describe their initial application to understand nonenzymatic solution reactions and reactions catalyzed by the enzyme ribonuclease A.



1. INTRODUCTION

The power of kinetic isotope effects (KIEs) combined with computation to resolve the mechanisms and characterize the transition states of enzymes is well established (Cook, 1991; Schramm, Horenstein, & Kline, 1994). However, measuring KIEs is extremely challenging due to their relatively small magnitude and the high precision that is usually required. Because of the wide range of substrates and chemical reactions catalyzed by enzymes, developing or adapting methods that allow transition-state analysis of key enzyme systems is a significant and continuing challenge. KIE analyses of enzymes that are current or potential therapeutic targets are particularly important since information on the catalytic transition states can provide guidelines for developing tight-binding competitive inhibitors (Schramm, 2015).

The breaking of RNA strands by 2'-*O*-transphosphorylation is a ubiquitous reaction in biology (Cuchillo, Nogues, & Raines, 2011; Oivanen, Kuusela, & Lonnberg, 1998), and enzymes that catalyze this reaction play key roles in RNA metabolism (Lilley, 2017; Masuda & Inouye, 2017; Saikia & Hatzoglou, 2015). Both protein ribonucleases and RNA enzymes (ribozymes) catalyze RNA strand cleavage by this mechanism making possible a comparison of biological catalysis by these two different polymers at a deep mechanistic level (Cochrane & Strobel, 2008; Lassila, Zalatan, & Herschlag, 2011; Wilcox, Ahluwalia, & Bevilacqua, 2011). The mechanisms of 2'-*O*-transphosphorylation in solution are relatively well studied, but they are complex and can involve different transition states depending on how the reaction is catalyzed (Kellerman, York, Piccirilli, & Harris, 2014; Korhonen, Koivusalo, Toivola, & Mikkola, 2013; Oivanen et al., 1998). Because of this complexity and the lack of experimental information on transition-state structure, pinning down the chemical details of enzyme-catalyzed RNA

strand cleavage has been difficult. Thus, developing experimental and computational methods for measuring and interpreting KIEs for solution RNA cleavage reactions and for ribonucleases and ribozymes presents an area where success can fill key gaps in our knowledge. Accordingly, we directed significant attention toward developing the experimental and conceptual framework for transition-state analysis of RNA reactions.

This chapter focuses on the details of the mass spectrometric methods used to measure $^{16}\text{O}/^{18}\text{O}$ ratios in substrate and/or product ribonucleotides. An essential component of transition-state analysis is computational simulation and calculations of predicted KIEs, e.g., (Harris, Piccirilli, & York, 2015; Vardi-Kilshtain, Nitoker, & Major, 2015; Wong, Xu, & Xu, 2015). Together the measurement and calculation of KIEs allow modeling of transition-state structure and permit different mechanistic possibilities to be evaluated. Computational methods are important for integrating KIE and other experimental data into a comprehensive mechanistic framework. Such a combination of theory and experiment has been essential for interpreting the KIEs measured for RNA cleavage reaction. The details of the computational methods used for developing transition-state models for RNA 2'-O-transphosphorylation are beyond the scope of this chapter. Nonetheless, such efforts are integral to success and we outline the resulting framework that has been thus developed for this class of reactions (Chen et al., 2014; Chen, Piccirilli, Harris, & York, 2015; Gu et al., 2013; Huang & York, 2014; Radak, Harris, & York, 2013; Wong et al., 2012). Finally, we discuss future questions that can be addressed regarding the mechanisms and transition states of RNA 2'-O-transphosphorylation reactions by applying the general approaches described herein.

1.1 Mechanisms and Transition States of RNA 2'-O-Transphosphorylation Reactions

Attack of the 2'OH nucleophile on the adjacent phosphoryl group results in a cyclic 2',3'-nucleotide monophosphate product and the adjacent nucleoside 5'-hydroxyl product (Fig. 1). There are large changes in the bonding and electron distribution around the 2'-O nucleophile, 5'-O leaving group, and nonbridging phosphoryl oxygens (NPOs) that may be probed by primary and secondary KIEs to gain insight into mechanism. Classic studies by Westheimer, Lönnberg, Cleland, and others established that phosphoryl transfer reactions can occur by a range of potential mechanisms and transition states (Breslow, 1993; Cleland & Hengge, 1995; Dennis & Westheimer, 1966; Kirby & Younas, 1970; Oivanen et al., 1998; Westheimer, 1968).

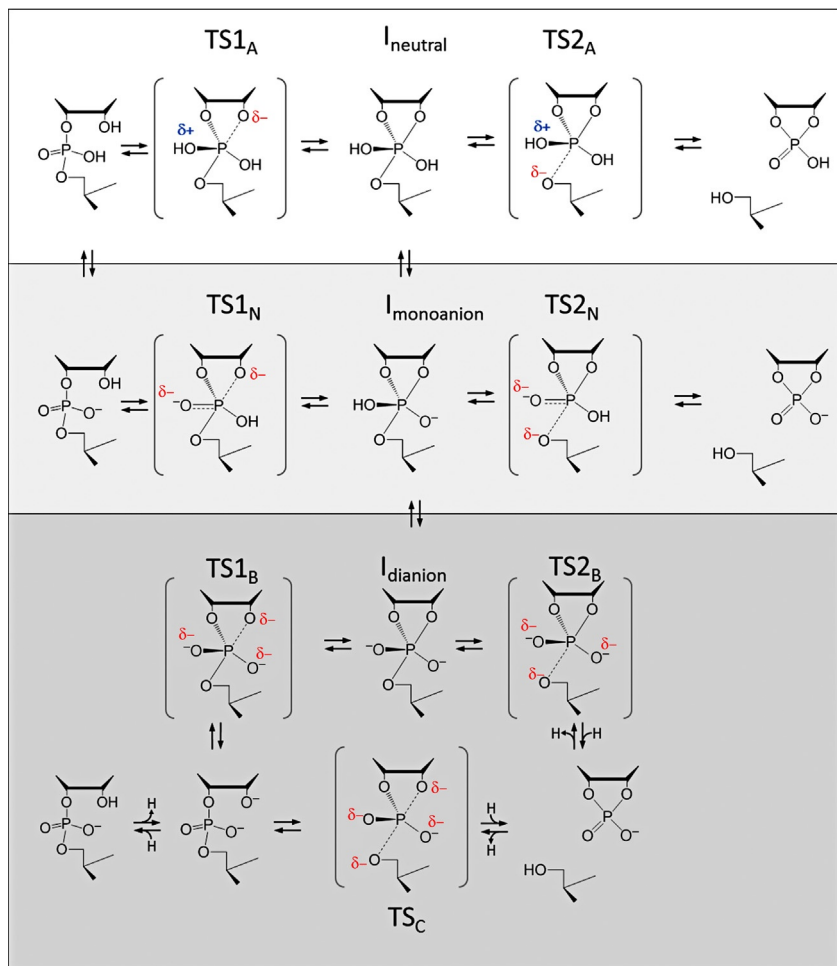


Fig. 1 Mechanisms and transition states for RNA 2'-O-transphosphorylation. (*Top*) Acid catalysis of neutral RNA and monoanion (*Middle*) by stepwise mechanisms via a neutral or monoanionic phosphorane. (*Bottom*) The stepwise (via a dianionic phosphorane) and concerted mechanisms for base catalysis.

Summarizing decades of research on the reactions of cyclic phosphodiester, we know that specific acid catalysis occurs by a stepwise mechanism involving the formation of a pentacoordinate phosphorane. The structure of the phosphorane may be neutral (I_{neutral}) or monoanionic ($I_{\text{monoanion}}$) depending on pH. Accordingly there are two separate transition states, one for nucleophilic attack (**TS1**) and another for leaving group departure (**TS2**). Formation of 2',5'-phosphodiester isomerization products, as observed for 2'-O-transphosphorylation reactions catalyzed by acid, is

characteristic of a mechanism in which the intermediate is in at least partial equilibrium with the substrate ground state and the rate-limiting transition state is TS2.

Specific base (OH^-) catalysis is typically depicted as occurring by a concerted mechanism with a single dianionic transition state (**TS_c**) (Cleland & Hengge, 1995; Gerratana, Sowa, & Cleland, 2000; Hengge, Bruzik, Tobin, Cleland, & Tsai, 2000; Oivanen et al., 1998). The KIE results obtained using the methods described herein helped to provide evidence that this is only true when the leaving group is “activated” (i.e., has a low $\text{p}K_{\text{a}}$), while those with a higher $\text{p}K_{\text{a}}$, e.g., the 5'-O of RNA, proceed by a stepwise mechanism through a dianionic phosphorane (**I_{dianion}**) in which **TS2** is rate limiting (Chen et al., 2014; Huang & York, 2014; Lonnberg, Stromberg, & Williams, 2004). In addition to this mechanistic complexity, phosphoryl transfer reactions necessarily involve proton transfers at the nucleophile, leaving group and potentially the NPOs. These transfers can either be concerted or occur in preequilibrium steps with respect to O–P bond formation/cleavage (i.e., they may occur by general or specific acid/base mechanisms (Jencks, 1987)). This overall framework, based on KIE and physical organic chemical studies, shows that acid/base and metal ion catalysis induce large effects on the structure of the rate-limiting TS (Cassano, Anderson, & Harris, 2004a; Humphry, Forconi, Williams, & Hengge, 2002, 2004; Humphry et al., 2008; Mikkola et al., 1999; Oivanen et al., 1998; Rawlings, Cleland, & Hengge, 2003; Rishavy, Hengge, & Cleland, 2000). The characteristic plasticity of phosphodiester cleavage mechanisms suggests both that the complex active site environments of enzymes are likely to alter TS structure, and that predicting the details of the mechanism by examining ground-state structures will be problematic.

Thus, the potential for KIE analyses to help resolve catalytic mechanisms of phosphoryl transfer enzymes is very high. This potential is founded on the extensive experimental and conceptual framework derived from analyses of the KIEs of phosphodiester reactions by the Hengge and Cleland labs (Cleland, 1982; Cleland & Hengge, 1995; Feng, Tanifum, Adams, Hengge, & Williams, 2009; Grzyska, Czyryca, Purcell, & Hengge, 2003; Hengge, 2002; Hengge, Aleksandra, & Cleland, 1995; Hengge et al., 2000; Rawlings, Cleland, & Hengge, 2006; Rishavy et al., 2000). Extensive studies of nucleophile, leaving group and nonbridging oxygen KIEs demonstrate that these effects fall in the range of 0.93–1.07 (k^{16}/k^{18}) and provide important information on extents of bond formation and cleavage (Cleland & Hengge, 2006; Hengge, 2002). Additionally, the equilibrium isotope effects

from the transfer of ionizable protons influence the observed KIEs. For example, the KIE for the nonbridging oxygens for hydrolysis of alkyl-nitrophenol phosphodiester is large and inverse in the acid-catalyzed reaction due to transfer of a proton. In contrast, a secondary nonbridging oxygen KIE of near unity is observed for late, product-like transition states of base-catalyzed reactions in which there is no proton transfer to these positions (Hengge, 2002; Hengge et al., 1995). Thus, KIE analysis of model diester reactions reveals relatively large and characteristic primary and secondary effects on the phosphoryl oxygens indicating that analogous studies can resolve details of RNA 2'-O-transphosphorylation transition-state structures.

1.2 Application of KIE Analyses to Investigate Transition States of RNA Strand Cleavage Reactions

In order to measure KIEs by internal competition, a mixed population of RNA isotopologues containing either ^{18}O or ^{16}O at a specific phosphoryl oxygen is allowed to react, and the change in isotopic composition of the residual substrate is analyzed. For example, to determine KIE on the nucleophile the 2'-O position must be site-specifically enriched with ^{18}O . For determination of KIEs on the 5'-O leaving group or nonbridging oxygens, different RNA isotopomers are required and these positions must be individually enriched in a different population of substrates. Typically, a level of enrichment near 50% in the substrate population is targeted so that the signal-to-noise ratio for the ^{16}O and ^{18}O isotopologues is essentially identical. As the reaction proceeds, the slower reacting isotopologue becomes progressively enriched in the unreacted substrate population, and the faster reacting isotopologue becomes progressively depleted. Analysis of the kinetics of the change in isotopic composition of unreacted RNA substrate as a function of reaction progress permits the KIE to be calculated by data fitting.

These kinds of experimental data report directly on differences in activation energy that reflect differences in bonding between the ground state and the transition state. However, interpretation of KIE data in terms of transition-state structure and bonding optimally requires the use of theoretical models. The necessary goal being to provide a direct connection between observed KIEs, as well as other physical biochemistry data (primarily Brønsted coefficients) measured for these reactions, with the structure and bonding in the transition state. Establishing such relationships is essential for evaluating mechanistic alternatives. Computational simulations offer a way to estimate the effects of different contributions to observed KIEs (such as protonation, changes in hybridization, metal ion coordination, and solvation) that may be difficult or impossible to measure experimentally.

In the present example, relationships between computation and experimental data have provided a powerful tool to investigate RNA phosphoryl transfer and demonstrate the utility of building up knowledge of mechanism through the systematic study of model systems to provide insight into more complex biological systems.



2. SYNTHESIS OF ISOTOPOMER RNA SUBSTRATES ENRICHED IN ^{18}O AT THE REACTING PHOSPHORYL OXYGENS

In order to measure primary KIEs on RNA 2'-O-transphosphorylation reactions, it is necessary to use different RNA isotopomers as substrates that are enriched with ^{18}O at the 2'-O (nucleophile) and 5'-O (leaving group) positions. The secondary KIEs at the NPO positions are also important, and RNAs enriched at these positions can provide key mechanistic information. Fig. 2 shows the oxygen atoms that can be interrogated using ^{18}O KIEs. The synthesis of isotopically enriched nucleotide monomers was recently reviewed by Weissman, Li, York, Harris, and Piccirilli (2015), and this contribution provides a comprehensive description of synthetic strategies to target key positions in the nucleobase and ribose. For synthetic purposes, the heavy and light nucleoside monomers are chemically equivalent; therefore, conversion to phosphoramidites and subsequent incorporation into RNA oligonucleotides utilizes standard methods. Of tremendous value for future studies is extensive literature on the synthesis of isotopically enriched nucleotides stemming from early work on nucleotide metabolism and classic stereochemical studies of phosphoryl transfer and enzyme catalysis (Brody & Frey, 1981; Connolly, Eckstein, & Fuldner, 1982; Jones, Kindman, & Knowles, 1978; Webb & Trentham, 1980). The ability to make these substrates, combined with the mass spectrometric methods outlined here provides a very powerful set of tools for analyzing a wide range of reactions and enzyme systems.

2.1 [2'- ^{18}O]Uridine

The synthesis of [2'- ^{18}O]uridine enables synthesis of RNA substrates for isotope effect analyses of nucleophilic activation by protein and RNA enzymes that catalyze RNA 2'-O-transphosphorylation. Uridine containing 2'- ^{18}O has been synthesized by reaction of commercially available and relatively inexpensive 2,2'-cyclouridine with an ^{18}O -enriched oxygen nucleophile that attacks the ribose C-2' regioselectively. As reported in Dai et al. potassium [$^{18}\text{O}_2$]benzoate favors ribose attack over nucleobase attack

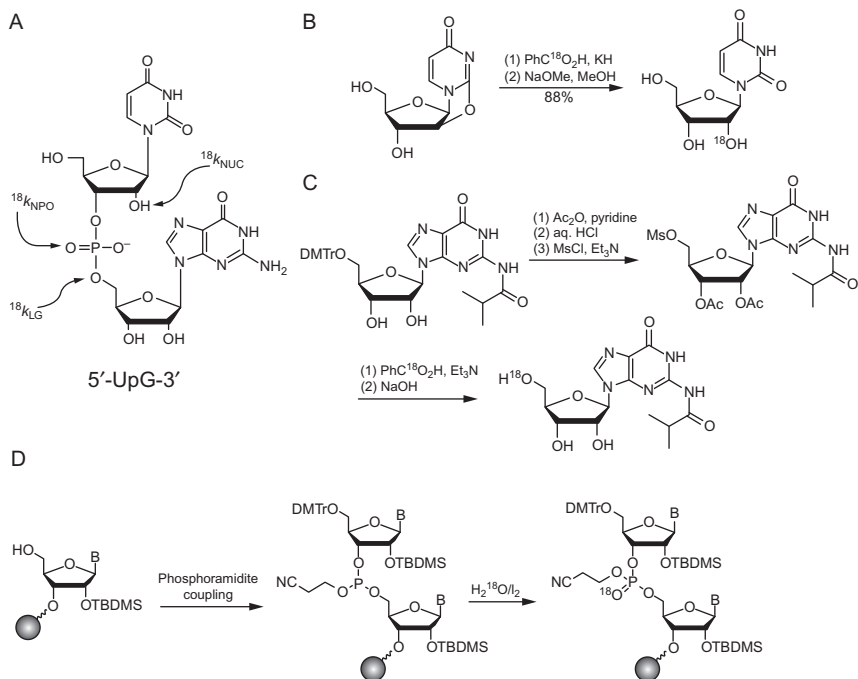


Fig. 2 (A) Structure of 5'-UpG-3' showing the locations of the isotopic enrichment with ^{18}O required to measure KIEs for the 2'-O nucleophile ($^{18}k_{\text{NUC}}$), 5'-O leaving group ($^{18}k_{\text{LG}}$), and nonbridging oxygens ($^{18}k_{\text{NPO}}$). (B) Scheme for synthesis of 2'-[^{18}O]uridine. (C) Scheme for synthesis of uridylyl-3'-guanosine-5'- ^{18}O -phosphate. (D) Scheme for synthesis of phosphoramidite. Panels (B–D) from Weissman, B. P., Li, N. S., York, D., Harris, M., & Piccirilli, J. A. (2015). Heavy atom labeled nucleotides for measurement of kinetic isotope effects. *Biochimica et Biophysica Acta*, 1854, 1737–1745.

on 2,2'-cyclouridine by 20-fold, thus allowing for efficient synthesis of [2'- ^{18}O]uridine and subsequently its phosphoramidite. This approach achieves high yield (88%) and employs a relatively inexpensive label source. The [$^{18}\text{O}_2$]benzoate is synthesized by acid hydrolysis of benzonitrile in $\text{HCl}/\text{H}_2^{18}\text{O}$. A mixture of [$^{18}\text{O}_2$]benzoic acid (1.0 equiv.) and potassium [$^{18}\text{O}_2$]benzoate (1.0 equiv.) at 140°C in DMF within 48 h gives products in a ratio of 20:1 ribo/arabino.

2.2 [5'- ^{18}O]Guanosine

Synthesis of [5'- ^{18}O]guanosine has been described previously in Gu et al. (2013). A similar strategy as that used for enrichment of the 2'-O position is employed to introduce ^{18}O using [$^{18}\text{O}_2$]benzoic acid to react with the

5'-O position. Commercially available 5'-DMT-*i*-Bu-guanosine is reacted and the 2' and 3' hydroxyls are protected with acetyl groups using standard methods. The 5'-DMT protecting group is subsequently removed by acid treatment. The 5'-hydroxyl is activated for nucleophilic attack as a mesylate ester, which is treated with [$^{18}\text{O}_2$]benzoic acid. The 5'-O-4,4-dimethoxytrityl (DMTr) protecting group is then added back resulting in a precursor compatible with phosphoramidite chemistry. As noted previously, this method should be generally applicable permitting all four 5'- ^{18}O -labeled nucleosides to be prepared with appropriate protection (Weissman et al., 2015).

2.3 [^{18}O] Incorporation Into NPOs

Labeling of the nonbridging oxygen positions is accomplished by adding H_2^{18}O during the oxidation step of solid-phase synthesis. Oxidation of phosphite triesters generates phosphate esters; using commercially available H_2^{18}O results in incorporation of the labeled oxygen at a nonbridging position. A drawback of this approach is that it generates the diastereomeric mixture of heavy atom substitution at either the pro- S_p or the pro- R_p . Thus, the observed $^{18}k_{\text{NPO}}$ reflects the contribution from both positions. It is worth noting that an overall advantage of the use of internal competition is that the isotopically enriched monomers described here are not required to be synthesized such that the incorporation of ^{18}O is 100%. As detailed later, the optimal ratio of heavy and light isotopologue substrates in the reaction is near 50/50 in order to achieve the highest degree of precision in the calculation of KIEs from MS data. Therefore, RNA isotopomers synthesized at higher levels of enrichment are necessarily diluted with natural abundance substrates that are also synthesized by standard phosphoramidite chemistry.

3. USE OF ELECTROSPRAY IONIZATION QUADRUPOLE/TIME-OF-FLIGHT MASS SPECTROMETRY TO MEASURE ^{18}O KIES FOR RNA 2'-O-TRANSPHOSPHORYLATION

3.1 Determination of Reaction Kinetics and Purification of Substrates and Products Using HPLC

The base-catalyzed 2'-O-transphosphorylation reaction of 5'-UpG-3' results in the formation of 2',3' cUMP and guanosine. Subsequent attack of hydroxide on the cyclic phosphate results in formation of a mixture of 2'-UMP and 3'-UMP. Acid catalysis occurs via a characteristic stepwise mechanism in which the phosphorane intermediate can rearrange and

subsequently decompose to the 2',5' phosphodiester isomer of UpG. The separation of nucleotides and RNA oligonucleotides by HPLC is well developed and offers multiple alternative approaches. For the reaction of 3',5'-UpG, the precursor dinucleotide as well as the guanosine, cUMP, and 2',5'-UpG isomerization products can all be separated and independently quantified using this approach.

The material requirement for a KIE experiment is fundamentally determined by the sensitivity of the isotope ratio measurement and secondarily by the chemical efficiency of the delivery of the substrate or product to be analyzed to the mass spectrometer. Determination of the sensitivity and precision of the isotope ratio measurement has to be evaluated for each analyte on each instrument. In our system, initial calibration experiments indicated that 100–200 pmol of UpG are sufficient to optimally measure $^{18}\text{O}/^{16}\text{O}$ ratios for KIE measurements. Therefore, in order to be able to take multiple time points at different fractions of reaction, a total of 1–5 nmol of UpG dinucleotide are typically used in each individual reaction. For solution reactions, the kinetics are first order in substrate concentration and therefore a concentration can be chosen convenient for subsequent sample workup and HPLC injection volume. The nonenzymatic solution reactions are sufficiently slow that simple neutralization and freezing is sufficient for quenching. For example, acid catalysis of UpG transphosphorylation at pH 0 was carried out in 250–500 μL at 37°C. Aliquots were removed at specific times in order to obtain fractions of reaction ranging from 0.1 to 0.7 and neutralized with an equivalent of NaOH followed by further dilution with 100–200 μL 0.1 M ammonium acetate pH 8.0. Ammonium acetate is used for the subsequent HPLC separation since it can be subsequently removed by lyophilization, which effectively desalts the sample to prepare it for electrospray ionization quadrupole/time-of-flight (ESI-Q/TOF).

RP-HPLC of nucleotides and short (<15-mer) oligonucleotides is widely used (Frederiksen & Piccirilli, 2009; Gilar, 2001; McLaughlin & Bischoff, 1987) and allows quantification of reaction progress and simultaneous purification for analysis of isotopic composition by ESI-Q/TOF with near quantitative recovery. Minor losses through incomplete injection of the reaction sample are inconsequential because the extent of reaction measurement and the isotopic measurement are both ratios and independent of the recovery. A Shimadzu Prominence HPLC system was used with detection at 260 and 254 nm coupled to a C18 column (300 \times 3.9 mm, 10 μm ; Phenomenex, Torrance, CA), eluting isocratically at 1 mL/min using a mobile phase of 0.1 M ammonium acetate containing 4% acetonitrile. Peaks

were identified using standards and analyses of UV absorbance and their areas were recorded and quantified using the manufacturer's software. Detection at two different wavelengths, 260 and 254 nm, identifies the position of the two mononucleoside products as these are the λ_{max} of uridine and guanosine, respectively. The difference in the A260 and A254 of the peaks eluting at 4 and 10 min is consistent with the identity of these species as cUMP and guanosine (Dawson, 1986).

The HPLC fractions containing the unreacted UpG are collected manually, taking care to collect the entire peak. In order to avoid fractionation due to interaction with the column, the collection begins before peak detection and continues until the remaining signal of the tail is well below 1% of the peak height as estimated by inspection of the signal as it is being collected. Since concentration of the sample is not difficult, there is no penalty for taking large (1–2 mL) total volumes. The lack of isotopic fractionation on this process can be demonstrated in initial experiments comparing values before and after chromatography. The recovered material is mixed, aliquoted into microfuge tubes containing <1 mL of volume, and dried by Speedvac without heating. The pellets are resuspended in 1 mL H₂O and dried down an additional four or more times to remove as much of the ammonium acetate salt as possible. The samples from each tube are progressively combined and concentrated. The recovered UpG is resuspended in water at a concentration of 20–50 μM for subsequent isotopic analysis by ESI-Q/TOF. It is important to check for further significant reaction during workup, which can easily be monitored by rechromatography of the UpG recovered from drying.

For determination of KIEs an important parameter for subsequent data fitting is the fraction of reaction, F/F_0 ($F = [P]/([P] + [S])$ and F_0 is this fraction calculated for a sample taken at $t=0$). Simple integration of the chromatogram permits quantification of reaction progress. This was done both with the Shimadzu integration software as well as by exporting the data and fitting it using Origin graphing and analysis software. The advantage of the latter is that it provides much more control over the setting of baselines. Comparison of the measured values to theoretical progress curves fit to the data allows the error in measurement to be estimated. As an example Fig. 3 shows the kinetics of acid-catalyzed 2'-O-transphosphorylation and isomerization. To confirm the precision of the determinations of F/F_0 these data are plotted vs time and fit to a standard exponential function and evaluation of the residuals tests whether the error in determination of F/F_0 is low. The data shown are for 3'-UpG-5' (filled squares), guanosine

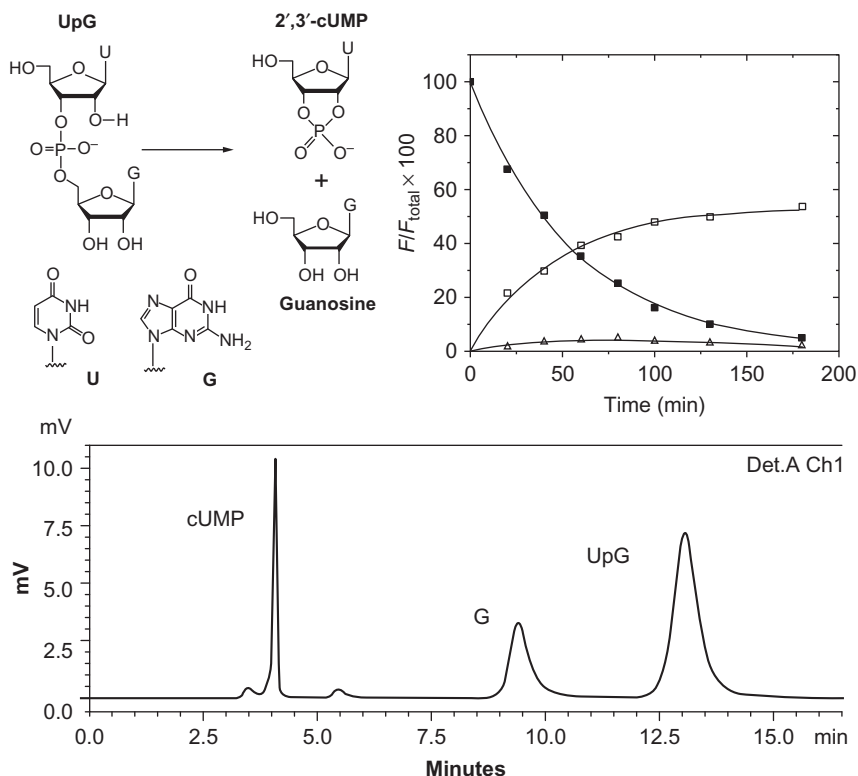


Fig. 3 (A) Scheme for 2'-*O*-transphosphorylation of 5'-UpG-3'. (B) HPLC chromatogram showing the separation of substrate (UpG) and products (cUMP and G). (C) Time course of changes in precursor and product species derived from integration of the corresponding peaks as illustrated in panel (B). The data shown are for 3'-UpG-5' (filled squares), guanosine (open squares), and the transient formation of the isomerization product 2'-UpG-5' is shown as open triangles. The cUMP product is not shown as it elutes in the void volume under these conditions and is difficult to quantify.

(open squares), and the transient formation of the isomerization product 2'-UpG-5' is shown as open triangles. The cUMP product is not shown as it elutes in the void volume under these conditions and is difficult to quantify.

Enrichment in the slower reacting isotopologue becomes progressively greater at higher F/F_0 . Since KIEs are typically only a few percent, the change in isotope ratio is measured in the residual substrate approximate this magnitude in the F/F_0 range of 0.2–0.9. This increase in signal to noise at high F/F_0 is advantageous; however, the error in determination of F/F_0 becomes increasingly greater at long reaction times as well since the signal

to noise in measurement of the low concentration of residual substrate approaches zero and the value for the product(s) approaches one. A zero, unreacted time point is taken for each reaction but, the isotope ratio in the starting population is not fixed as a constant in the determination of KIEs. By fitting the data with the ratio at time = 0 as a variable rather than fixing it as a constant using the measured value, this single measurement of $^{16}\text{O}/^{18}\text{O}$ is not unduly weighted in the data fitting.

3.2 Determination of $^{16}\text{O}/^{18}\text{O}$ Ratios in 5'-UpG-3' by Tandem Q/TOF MS

The high precision required for KIE measurements has been achieved using isotope ratio mass spectrometry (IRMS) or dual-label scintillation counting of radioactive isotopes (Hengge & Cleland, 1991). While these methods have proven highly informative in deciphering enzyme transition states, both possess inherent limitations that restrict their application. IRMS can only analyze small, nonpolar gasses and scintillation counting requires double-labeling schemes involving specific isotopic pairs limiting the molecules that can be analyzed. One alternative to these methods is whole molecule mass spectrometry using electrospray ionization (ESI) or matrix-assisted laser desorption ionization to allow larger molecules to be analyzed.

Coupled with QMS, ESI makes possible the analysis of isotope ratios for numerous biologically relevant organic molecules with molecular masses in excess of 500 Da and application has allowed KIEs to be determined for peptidyl transfer and RNA hydrolysis. However, several features limit the precision and accuracy of QMS. These features include noise (from both the ion source and detector), background, intensity fluctuations, and the inability to capture the entire ion current arising from individual isotopologues. These effects can be minimized by working with isotope ratios near unity, utilizing background subtraction, and/or injecting analyte by continuous direct infusion. Previously, we showed that the data necessary to calculate isotope effects as small as 1.005 could be obtained by analytically integrating intensity vs m/z data obtained by ESI-QMS to determine the isotope ratios (Cassano et al., 2007). The ability to analyze isotope ratios in nucleotides permitted the application of heavy atom isotope effect studies to RNA hydrolysis demonstrating attack by hydroxide ion and metal ion catalysis by direct coordination (Cassano, Anderson, & Harris, 2002, 2004a, 2004b).

Fundamentally, the degree of mechanistic information that can be obtained is limited by precision, which in turn is limited by the MS component of the analysis. In this regard, the use of tandem Q/TOF MS with the same ESI mode of ion generation presents several potentially transformative advantages. The TOF acquisition by design generates data in profile mode, in which the intensity over a range of m/z values is plotted, allowing all of the isotopomers in a cluster to be quantitatively analyzed. Also, the tandem approach has much greater signal to noise since the background of the second TOF dimension is essentially zero. Additionally, with increased sensitivity and the ability to perform long acquisition times, many individual scans can be averaged which results in a corresponding increase in precision. Also, as described in more detail later the KIE can be determined from multiple fragment ions from the same molecule which provides a check on internal accuracy. The higher sensitivity and throughput, together with analyses of multiple fragment ions allow comparison of multiple independent determinations and allow KIEs to be measured with precision approaching ± 0.001 . Application of ESI-Q/TOF imposes several requirements: (1) product ions are generated that contain the isotopically labeled oxygen, (2) the isotope ratio can be measured with sufficient precision that standard errors in data fitting to determine KIE are low, and (3) the experimental error is sufficiently low that mechanistic interpretations can be made.

The first requirement is demonstrated by the TOF mass spectrum of the product ions of $m/z = 588$ (Fig. 4). In this experiment, the solution to be analyzed was injected by automated syringe pump at a flow rate of $1 \mu\text{L}/\text{min}$ and the UpG ion was identified in a single dimension of TOF MS and a mass range encompassing the entire isotopic envelope was selected. In practice, this is done empirically by varying the m/z range of the quadrupole isolation until the isotope ratio in the product ions is constant. Fragments are generated by inert gas collision with collision energies of ca. 35 V, and the resultant molecules are separated by a second dimension of TOF MS.

Fig. 4 shows a scan of ion intensity and the resultant fragment ions analyzed by TOF MS. Fragmentation of UpG gives rise to ions at 476, 362, 305, 255, 211, 192, and 111 amu. To optimize the generation of these ions the collision energy was varied and the ion intensity quantified. The 255 amu ion was present in the unfragmented spectrum and varied in intensity and does not contain any of the enriched positions. For these reasons, this ion was considered to be a contaminant and was not analyzed further. Since the $^{16}\text{O}/^{18}\text{O}$ at the 2'-O of UpG is ~ 1.0 in this experiment, the resulting

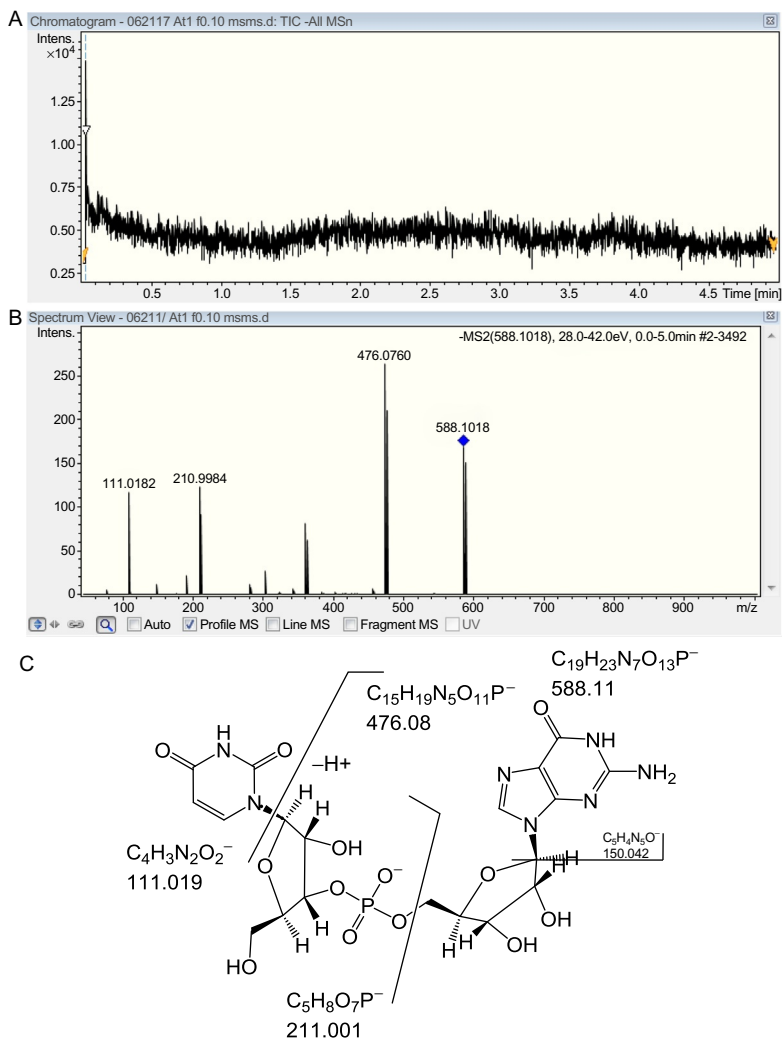


Fig. 4 (A) Total ion current time course of the direct infusion of UpG. *Shaded area* indicates the time span averaged to generate the mass spectrum. (B) Averaged negative ion tandem mass spectrum of the isotopic cluster around m/z . The insets demonstrate the resolution, peak shape, and lack of background signal around m/z 211 and 476. (C) Fragmentation products of UpG. The elemental composition and monoisotopic masses of the fragment ions are given.

product ions that contain the labeled oxygen can be identified by the pattern observed in their isotopic cluster. Only the 476, 305, 211, and 193 ions contain the enriched 2'-hydroxyl as expected from the structures of these molecules (Fig. 4). Of these fragmentation products the signal to noise of the 476

and 211 ions is clearly greater and these ions were selected for further quantitative analysis. Fortunately, both ions also contain the 5'-O and NBOs and therefore are useful for determination of KIEs at all of the reacting phosphoryl oxygens. The peak shapes are largely symmetrical and the area can be integrated manually, or by using the routines included in the software (Analyst, ABI).

While all of the ions are derived from the same population in this analyzed solution, the isotope ratios determined by ESI-Q/TOF are significantly different. For example, at a collision energy of 35 the ratios for the 588, 476, and 211 ions were determined to be 1.08, 1.14, and 1.35, respectively. Clearly, the accuracy of the ratios is suspect since each are derived from the same isotopologue population. Evidence that the difference in the ratios is due to effects arising from collision is shown in Fig. 5. In this example, the observed ratio was monitored over a range of collision energies. Interestingly, the ratio varies by as much as 20% for all of the ions as the collision energy is raised. This sensitivity to collision energy suggests that subtle effects on ion flight are responsible for these differences. Multiple collisions may result in progressive displacement of the lighter ion from the ion path. For the 211 ion, at some level this displacement must result in enrichment of the secondary 211 ion. This makes sense since at higher collision energies the ^{18}O -enriched 476 ion population resulting from by multiple collisions begins to decay to the 211 ion. Therefore, the accuracy of the ratios is relatively low and as an analytic method to determine ratios of unknowns, much additional work would be necessary to establish the source of these variations.

However, for isotope effect determinations using competitive methods the absolute accuracy of the measurements is not an important factor. In the determination of the isotope effect, the same inaccuracy will be present in all of the data points analyzed. The key issue is whether changes in the ratio can be determined with sufficient precision to follow the enrichment of one or the other of the isotopologues as a function of reaction progress. To assess the precision with which $^{16}\text{O}/^{18}\text{O}$ ratios may be measured in UpG using this method, we compared the observed ratio to the ratio predicted from a set of control samples that were progressively diluted with natural abundance UpG. Fig. 5 shows a linear plot of the observed vs predicted ratio. The linearity of the data ($R^2 > 0.95$) demonstrates the ability of the method to discriminate changes in the observed ratio that is well within the precision required for KIE calculation. One factor necessary to maintain discriminate precise differences between successive samples, is to take care to minimize sample bleedover effects. Residual sample in the injector lines, sample inlet,

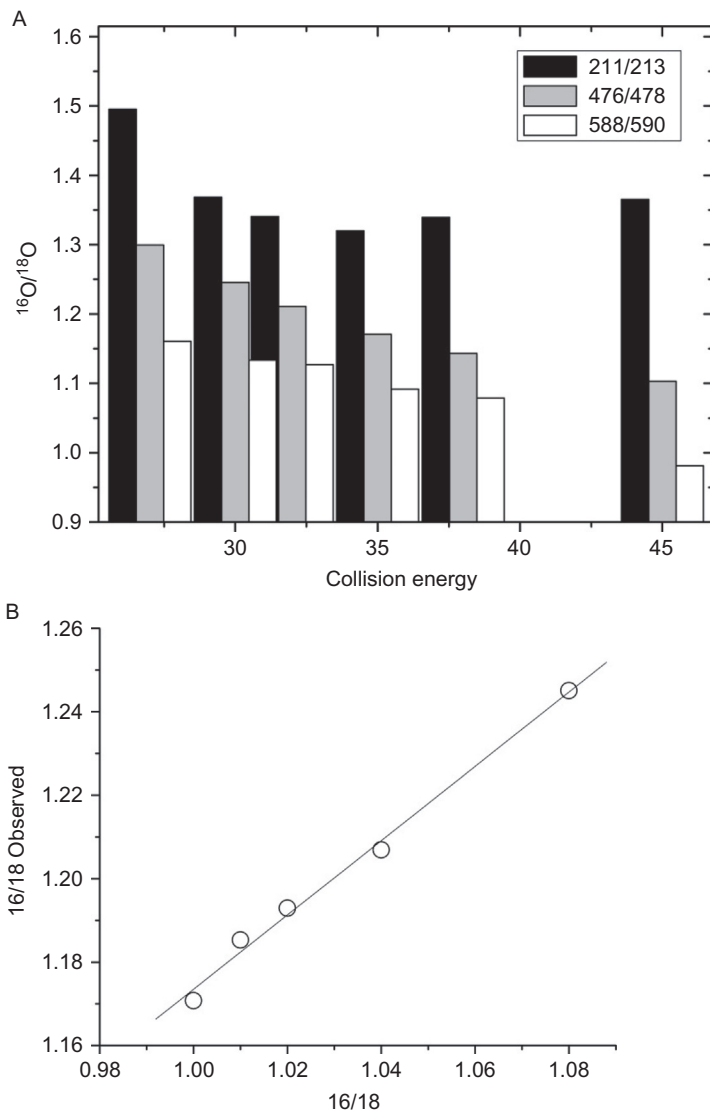


Fig. 5 (A) Bar graph showing the dependence on collision energy (V) of the observed $^{16}\text{O}/^{18}\text{O}$ ratio calculated from the Q/TOF MS analysis of fragments shown in Fig. 4. (B) Comparison of the intrinsic vs observed $^{16}\text{O}/^{18}\text{O}$ ratios for UpG determined from the 211 m/z fragment.

and ionization cell can result in significant contributions to the observed signal if these components are not sufficiently rinsed between samples. It is necessary to monitor background to insure that no bleedover will occur during acquisition of the subsequent sample.

3.3 Data Fitting and Calculation of KIEs Using Internal Competition Kinetics

To determine the isotope effect the natural log of the ratio measurements are plotted vs the fraction of reaction. Fig. 6 shows the results for determination of the KIE on the nonbridging oxygen for the acid-catalyzed 2'-*O*-transphosphorylation reaction of the UpG dinucleotide. These data are fit to the following equation:

$$\ln(R_s) = (1/^{18}k - 1) \ln(1 - F) + \ln(R_0) \quad (1)$$

where ^{18}k is the isotope effect, F is the fraction of unreacted (residual) substrate (UpG) quantified by RP-HPLC, and R_s and R_0 are the ratios of $^{16}\text{O}/^{18}\text{O}$ for the unreacted substrate at F and its initial value, respectively. Eq. (1) is derived from internal competition kinetics and is used for fitting the precursor ratio. The derivation of this expression as well as the background and equations for fitting product ratios has recently been reviewed (Anderson, 2015).

Table 1 shows the compiled results from three independent experimental determinations of $^{18}k_{\text{NBO}}$. The increase in sensitivity permits an individual determination to be made using ca. 0.5 nmol of enriched nucleotide substrate, and thus multiple determinations can be made with a relatively small investment of material compared to previous whole molecule analyses and IRMS. Since the MS analysis allows the ratio to be determined in both the 211 and 476 ions each experiment yields two independent determinations of the isotope effect. Importantly, essentially the same KIE is measured whether the 211 or 476 ion is used for the analysis (see later). For each experiment, a duplicate reaction was run and thus each experiment results in four determinations of the KIE from data fitting for a total of 12 measurements of $^{18}k_{\text{NBO}}$. Averaging with equal weighting yields a value of 0.9944 ± 0.0074 . A threshold for inclusion of individual experiments can be set if necessary at a standard error of <0.005 for determination of the KIE by fitting isotope ratio vs reaction progress data. Evaluation of the reaction kinetics can also be used to identify determinations in which the accuracy is questionable. Goodness of fit can be used as a criterion to exclude outlier data and can also be used to weight the individual KIE determinations. In this operation the individual KIEs are multiplied by the reciprocal of the standard error, averaged, and then divided by the sum of the reciprocals. If the values are weighted in this fashion and all measurements are included the $^{18}k_{\text{NBO}}$ is determined to be 0.9907 ± 0.0012 . Given this data set the computed $^{18}k_{\text{NBO}}$ from using either

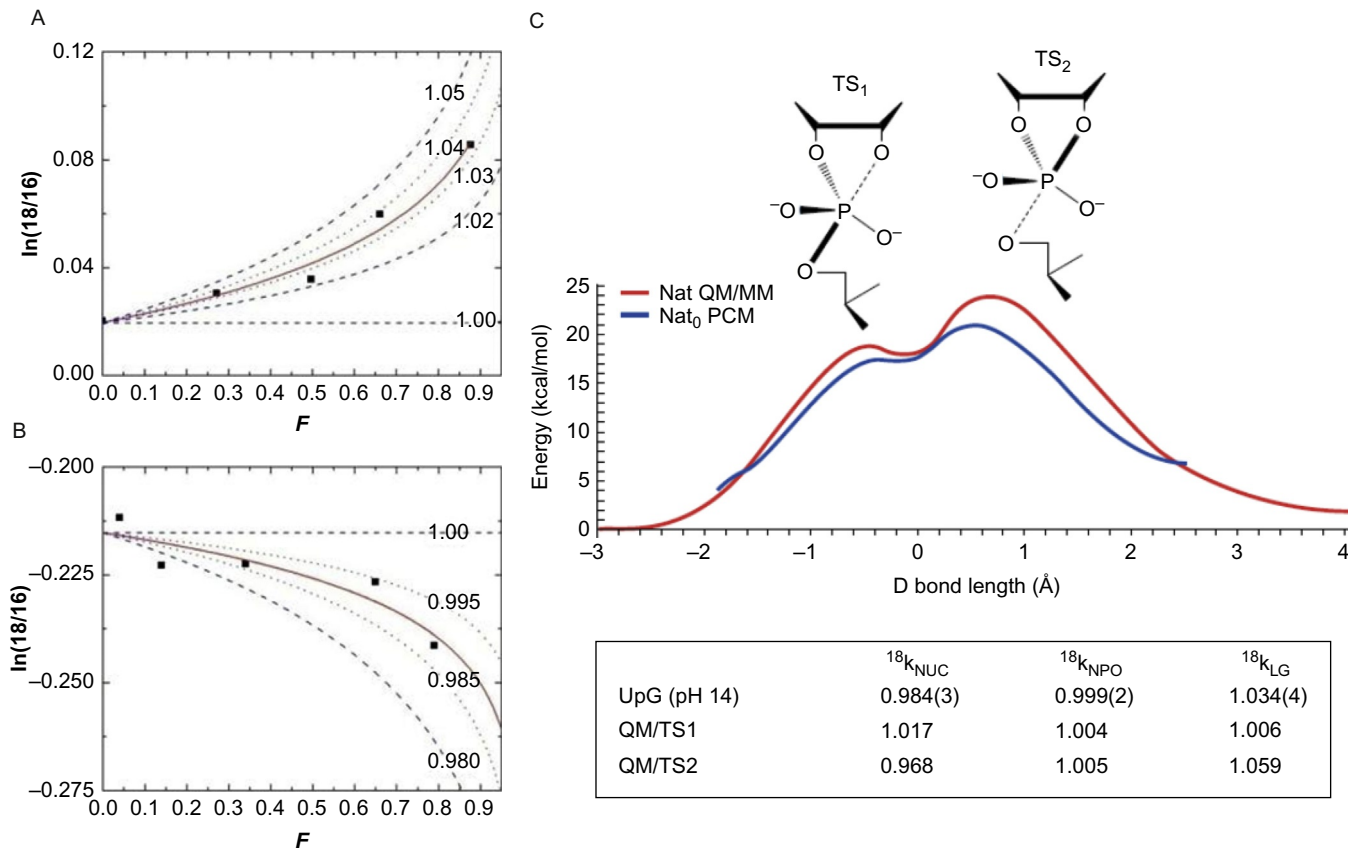


Fig. 6 Determination of observed KIEs by analysis of $\ln(^{16}\text{O}/^{18}\text{O})$ vs F data. (A) Determination of $^{18}k_{\text{LG}}$ by quantification of the change in $^{16}\text{O}/^{18}\text{O}$ as a function of reaction progress (*filled symbols*). The *red line* is a fit of the data to Eq. (1) yielding a KIE of 1.032. The *blue lines* represent simulations that span the range of observable ^{18}O KIEs. (B) Determination of $^{18}k_{\text{NUC}}$. The data and fit to Eq. (1) are indicated as in panel A. The *blue lines* represent simulations of KIEs of unity to 0.980 inverse for comparison. (C) Comparison of density-functional QM/MM free energy and adiabatic PCM profiles for the native 2'-*O*-transphosphorylation reaction as a function of the difference of the bond distance (Δ bond distance) between the breaking bond P-O5' and the forming bond P-O2'. Examples of the observed and calculated KIEs for TS1 and TS2 are shown.

Table 1 Independent Determinations of $^{18}k_{\text{NBO}}$

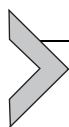
	$^{18}k_{\text{NB}}$	Std Error
Experiment-001		
Reaction-A 211 ion	0.9914	0.00189
Reaction-A 476 ion	0.991	0.00172
Reaction-B 211 ion	0.9911	0.00162
Reaction-B 476 ion	0.99121	0.00145
Experiment-002		
Reaction-A 211 ion	0.99228	0.00439
Reaction-A 476 ion	0.99136	0.0045
Reaction-B 211 ion	1.0093	0.01585
Reaction-B 476 ion	1.011	0.01914
Experiment-003		
Reaction-A 211 ion	0.9915	0.00123
Reaction-A 476 ion	0.98901	0.000205
Reaction-B 211 ion	0.9924	0.00095
Reaction-B 476 ion	0.9913	0.000239

the 211 or the 476 amu data alone can be compared. If only the 211 data is used the $^{18}k_{\text{NBO}}$ is found to be 0.991736 ± 0.000572 and if only the 476 data is used the $^{18}k_{\text{NBO}}$ is 0.990776 ± 0.000997 . Importantly, use of either ion gives essentially the same value for $^{18}k_{\text{NBO}}$ within 0.001 and with comparable precision. These results indicate that the method is robust and that the inaccuracies in the observed isotope ratios do not influence the measured KIE and serve as an excellent check on internal accuracy in determination of the effect.

The cleavage of RNA chains by attack of the adjacent 2'-OH is universal in biology and has been intensively studied since the 1950s, yet these approaches allow the first characterization of RNA cleavage with primary isotope effects capable of directly informing on the extent of bond cleavage in the transition state. Comparing the results with the literature and KIE measurements of model phosphoryl transfer reactions reveals that significant differences exist in the transition states for concerted phosphoryl transfer

reactions and that the high pK_a of the leaving group coupled with the enforced geometry of cleavage can significantly alter the transition state for the reaction. The KIE data indicate a concerted mechanism in which bond formation to the nucleophile and bond cleavage from the leaving group are both advanced in a “late” or product-like transition state. The nucleophile isotope effects implicate equilibrium deprotonation of the 2'-O prior to nucleophilic attack, and thus catalysis by hydroxide occurs by a specific base mechanism.

As reported in Wong et al., the density-functional QM/MM free energy profile and the PCM adiabatic reaction profile for the reaction of the native compound are very similar (Fig. 6) (Wong et al., 2012). Both profiles show an associative mechanism with distinct TS1 and TS2 transition states that are separated by a shallow, metastable intermediate (I_{dianion}). In both cases, TS2 is rate controlling. Importantly, TS2 has considerable “late” character, in which cleavage of the exocyclic P-O5' bond is advanced. The calculated density-functional free energy barrier with PCM solvation is very similar to that estimated from the experimental rate for UpG transphosphorylation (ca. 20 kcal mol⁻¹). This result, along with the consistent values from the PCM reaction profile and from the QM/MM simulations with explicit solvent, suggests that the density-functional PCM calculations sufficiently capture the essential features of the solvation effects on the reaction profile to determine the KIE values (Chen et al., 2014; Radak et al., 2013; Wong et al., 2012). Thus, taken together the results provide an atomic-level picture of the reactions, which includes a detailed characterization of the rate-controlling transition state for RNA transphosphorylation.



4. FUTURE DIRECTIONS

An important step is application of these methods to enzymes including both protein ribonucleases and small self-cleavage ribozymes. Indeed, we have reported initial application to RNase A catalysis (Gu et al., 2013) and the results and implications for catalytic mechanism have been recently reviewed (Harris et al., 2015; Kellerman et al., 2014). The transition state analyses of RNase A represent an initial first step, but illustrate the complexity of measuring KIEs for enzymes. Unlike solution reactions, an important consideration for enzyme reactions is the determination of substrate-binding commitments, which can obscure the intrinsic magnitude of KIEs on the chemical step. A complete treatment of these factors as they apply to RNase A and other ribonucleases is beyond the scope of this

chapter. However, it is apparent that the early success with RNase A bodes extremely well for application to additional systems. RNA endonucleases such as bacterial ribotoxins and ribonucleases involved in modulating gene expression are important future targets. Information about the transition states for these enzymes can potentially provide inroads into the development of transition state-based inhibitors. On a technical level, the advent of mass spectrometers that permit very high-resolution mass resolution, or atomic fine structure, raises new possibilities for isotope ratio determinations. The information gained over the course of such studies is highly likely to have broad impact by enabling the improvement of computational methods, facilitating the design of novel catalysts, and revealing the potential for development of transition state based inhibitors.

REFERENCES

- Anderson, V. E. (2015). Multiple alternative substrate kinetics. *Biochimica et Biophysica Acta*, 1854, 1729–1736.
- Breslow, R. (1993). Kinetics and mechanism in RNA cleavage. *Proceedings of the National Academy of Sciences of the United States of America*, 90, 1208–1211.
- Brody, R. S., & Frey, P. A. (1981). Unambiguous determination of the stereochemistry of nucleotidyl transfer catalyzed by DNA polymerase I from *Escherichia coli*. *Biochemistry*, 20, 1245–1252.
- Cassano, A. G., Anderson, V. E., & Harris, M. E. (2002). Evidence for direct attack by hydroxide in phosphodiester hydrolysis. *Journal of the American Chemical Society*, 124, 10964–10965.
- Cassano, A. G., Anderson, V. E., & Harris, M. E. (2004a). Analysis of solvent nucleophile isotope effects: Evidence for concerted mechanisms and nucleophilic activation by metal coordination in nonenzymatic and ribozyme-catalyzed phosphodiester hydrolysis. *Biochemistry*, 43, 10547–10559.
- Cassano, A. G., Anderson, V. E., & Harris, M. E. (2004b). Understanding the transition states of phosphodiester bond cleavage: Insights from heavy atom isotope effects. *Biopolymers*, 73, 110–129.
- Cassano, A. G., Wang, B., Anderson, D. R., Previs, S., Harris, M. E., & Anderson, V. E. (2007). Inaccuracies in selected ion monitoring determination of isotope ratios obviated by profile acquisition: Nucleotide 18O/16O measurements. *Analytical Biochemistry*, 367, 28–39.
- Chen, H., Giese, T. J., Huang, M., Wong, K. Y., Harris, M. E., & York, D. M. (2014). Mechanistic insights into RNA transphosphorylation from kinetic isotope effects and linear free energy relationships of model reactions. *Chemistry—A European Journal*, 20(44), 14336–14343.
- Chen, H., Piccirilli, J. A., Harris, M. E., & York, D. M. (2015). Effect of Zn binding and enzyme active site on the transition state for RNA 2'-O-transphosphorylation interpreted through kinetic isotope effects. *Biochimica et Biophysica Acta*, 1854(11), 1795–1800.
- Cleland, W. W. (1982). Use of isotope effects to elucidate enzyme mechanisms. *CRC Critical Reviews in Biochemistry*, 13, 385–428.
- Cleland, W. W., & Hengge, A. C. (1995). Mechanisms of phosphoryl and acyl transfer. *FASEB Journal*, 9, 1585–1594.

- Cleland, W. W., & Hengge, A. C. (2006). Enzymatic mechanisms of phosphate and sulfate transfer. *Chemical Reviews*, *106*, 3252–3278.
- Cochrane, J. C., & Strobel, S. A. (2008). Catalytic strategies of self-cleaving ribozymes. *Accounts of Chemical Research*, *41*, 1027–1035.
- Connolly, B. A., Eckstein, F., & Fuldner, H. H. (1982). Stereospecific substitution of oxygen-18 for sulfur in nucleoside phosphorothioates. *The Journal of Biological Chemistry*, *257*, 3382–3384.
- Cook, P. F. (1991). *Enzyme mechanism from isotope effects*. New York: CRC Press.
- Cuchillo, C. M., Nogues, M. V., & Raines, R. T. (2011). Bovine pancreatic ribonuclease: Fifty years of the first enzymatic reaction mechanism. *Biochemistry*, *50*, 7835–7841.
- Dawson, R. M. C. (1986). *Data for biochemical research*. Oxford, UK: Clarendon Press.
- Dennis, E. A., & Westheimer, F. H. (1966). The geometry of the transition state in the hydrolysis of phosphate esters. *Journal of the American Chemical Society*, *88*, 3432–3433.
- Feng, G., Tanifum, E. A., Adams, H., Hengge, A. C., & Williams, N. H. (2009). Mechanism and transition state structure of aryl methylphosphonate esters doubly coordinated to a dinuclear cobalt(III) center. *Journal of the American Chemical Society*, *131*, 12771–12779.
- Frederiksen, J. K., & Piccirilli, J. A. (2009). Separation of RNA phosphorothioate oligonucleotides by HPLC. *Methods in Enzymology*, *468*, 289–309.
- Gerratana, B., Sowa, G. A., & Cleland, W. W. (2000). Characterization of the transition state structures and mechanisms for the isomerization and cleavage reactions of 3'-m-nitrobenzyl phosphate. *Journal of the American Chemical Society*, *122*, 12615–12621.
- Gilar, M. (2001). Analysis and purification of synthetic oligonucleotides by reversed-phase high-performance liquid chromatography with photodiode array and mass spectrometry detection. *Analytical Biochemistry*, *298*, 196–206.
- Grzyska, P. K., Czryca, P. G., Purcell, J., & Hengge, A. C. (2003). Transition state differences in hydrolysis reactions of alkyl versus aryl phosphate monoester monoanions. *Journal of the American Chemical Society*, *125*, 13106–13111.
- Gu, H., Zhang, S., Wong, K. Y., Radak, B. K., Dissanayake, T., Kellerman, D. L., et al. (2013). Experimental and computational analysis of the transition state for ribonuclease A-catalyzed RNA 2'-O-transphosphorylation. *Proceedings of the National Academy of Sciences of the United States of America*, *110*, 13002–13007.
- Harris, M. E., Piccirilli, J. A., & York, D. M. (2015). Integration of kinetic isotope effect analyses to elucidate ribonuclease mechanism. *Biochimica et Biophysica Acta*, *1854*, 1801–1808.
- Hengge, A. C. (2002). Isotope effects in the study of phosphoryl and sulfuryl transfer reactions. *Accounts of Chemical Research*, *35*, 105–112.
- Hengge, A. C., Aleksandra, T. E., & Cleland, W. W. (1995). Studies of transition-state structures of phosphoryl transfer reactions of phosphodiester of p-nitrophenol. *Journal of the American Chemical Society*, *117*, 5919–5926.
- Hengge, A. C., Bruzik, K. S., Tobin, A. E., Cleland, W. W., & Tsai, M. D. (2000). Kinetic isotope effects and stereochemical studies on a ribonuclease model: Hydrolysis reactions of uridine 3'-nitrophenyl phosphate. *Bio-Organic Chemistry*, *28*, 119–133.
- Hengge, A. C., & Cleland, W. W. (1991). Phosphoryl-transfer reactions of phosphodiester: Characterization of transition states by heavy-atom isotope effects. *Journal of the American Chemical Society*, *113*, 5835–5841.
- Huang, M., & York, D. M. (2014). Linear free energy relationships in RNA transesterification: Theoretical models to aid experimental interpretations. *Physical Chemistry Chemical Physics*, *16*, 15846–15855.
- Humphry, T., Forconi, M., Williams, N. H., & Hengge, A. C. (2002). An altered mechanism of hydrolysis for a metal-complexed phosphate diester. *Journal of the American Chemical Society*, *124*, 14860–14861.

- Humphry, T., Forconi, M., Williams, N. H., & Hengge, A. C. (2004). Altered mechanisms of reactions of phosphate esters bridging a dinuclear metal center. *Journal of the American Chemical Society*, *126*, 11864–11869.
- Humphry, T., Iyer, S., Iranzo, O., Morrow, J. R., Richard, J. P., Paneth, P., et al. (2008). Altered transition state for the reaction of an RNA model catalyzed by a dinuclear zinc(II) catalyst. *Journal of the American Chemical Society*, *130*, 17858–17866.
- Jencks, W. P. (1987). *Catalysis in chemistry and enzymology*. New York: Dover Publications.
- Jones, S. R., Kindman, L. A., & Knowles, J. R. (1978). Stereochemistry of phosphoryl group transfer using a chiral [16O, 17O, 18O] stereochemical course of alkaline phosphatase. *Nature*, *275*, 564–565.
- Kellerman, D. L., York, D. M., Piccirilli, J. A., & Harris, M. E. (2014). Altered (transition) states: Mechanisms of solution and enzyme catalyzed RNA 2'-O-transphosphorylation. *Current Opinion In Chemical Biology*, *21*, 96–102.
- Kirby, A. J., & Younas, M. (1970). The reactivity of phosphate esters. Reactions of diesters with nucleophiles. *Journal of the Chemical Society B: Physical Organic*, *B*, 1165–1172.
- Korhonen, H., Koivusalo, T., Toivola, S., & Mikkola, S. (2013). There is no universal mechanism for the cleavage of RNA model compounds in the presence of metal ion catalysts. *Organic & Biomolecular Chemistry*, *11*, 8324–8339.
- Lassila, J. K., Zalatan, J. G., & Herschlag, D. (2011). Biological phosphoryl-transfer reactions: Understanding mechanism and catalysis. *Annual Review of Biochemistry*, *80*, 669–702.
- Lilley, D. M. J. (2017). How RNA acts as a nuclease: Some mechanistic comparisons in the nucleolytic ribozymes. *Biochemical Society Transactions*, *45*, 683–691.
- Lonnberg, H., Stromberg, R., & Williams, A. (2004). Compelling evidence for a stepwise mechanism of the alkaline cyclisation of uridine 3'-phosphate esters. *Organic & Biomolecular Chemistry*, *2*, 2165–2167.
- Masuda, H., & Inouye, M. (2017). Toxins of prokaryotic toxin-antitoxin systems with sequence-specific endoribonuclease activity. *Toxins*, *9*, 1–23.
- McLaughlin, L. W., & Bischoff, R. (1987). Resolution of RNA using high-performance liquid chromatography. *Journal of Chromatography*, *418*, 51–72.
- Mikkola, S., Stenman, E., Nurmi, K., Yousefi-Salakdeh, E., Stromberg, R., & Lonnberg, H. (1999). The mechanism of the metal ion promoted cleavage of RNA phosphodiester bonds involves a general acid catalysis by the metal aquo ion on the departure of the leaving group. *Journal of the Chemical Society, Perkin Transactions*, *2*, 1619–1625.
- Oivanen, M., Kuusela, S., & Lonnberg, H. (1998). Kinetics and mechanism for the cleavage and isomerization of phosphodiester bonds of RNA by Bronsted acids and bases. *Chemical Reviews*, *98*, 961–990.
- Radak, B. K., Harris, M. E., & York, D. M. (2013). Molecular simulations of RNA 2'-O-transesterification reaction models in solution. *The Journal of Physical Chemistry. B*, *117*, 94–103.
- Rawlings, J., Cleland, W. W., & Hengge, A. C. (2003). Metal ion catalyzed hydrolysis of ethyl p-nitrophenyl phosphate. *Journal of Inorganic Biochemistry*, *93*, 61–65.
- Rawlings, J., Cleland, W. W., & Hengge, A. C. (2006). Metal-catalyzed phosphodiester cleavage: Secondary 18O isotope effects as an indicator of mechanism. *Journal of the American Chemical Society*, *128*, 17120–17125.
- Rishavy, M. A., Hengge, A. C., & Cleland, W. W. (2000). Lanthanide catalyzed cyclization of uridine 3'-p-Nitrophenyl phosphate. *Bio-Organic Chemistry*, *28*, 283–292.
- Saikia, M., & Hatzoglou, M. (2015). The many virtues of tRNA-derived stress-induced RNAs (tiRNAs): Discovering novel mechanisms of stress response and effect on human health. *The Journal of Biological Chemistry*, *290*, 29761–29768.
- Schramm, V. L. (2015). Transition states and transition state analogue interactions with enzymes. *Accounts of Chemical Research*, *48*, 1032–1039.

- Schramm, V. L., Horenstein, B. A., & Kline, P. C. (1994). Transition state analysis and inhibitor design for enzymatic reactions. *The Journal of Biological Chemistry*, *269*, 18259–18262.
- Vardi-Kilshain, A., Nitoker, N., & Major, D. T. (2015). Nuclear quantum effects and kinetic isotope effects in enzyme reactions. *Archives of Biochemistry and Biophysics*, *582*, 18–27.
- Webb, M. R., & Trentham, D. R. (1980). Analysis of chiral inorganic [16O, 17O, 18O] thiophosphate and the stereochemistry of the 3-phosphoglycerate kinase reaction. *The Journal of Biological Chemistry*, *255*, 1775–1778.
- Weissman, B. P., Li, N. S., York, D., Harris, M., & Piccirilli, J. A. (2015). Heavy atom labeled nucleotides for measurement of kinetic isotope effects. *Biochimica et Biophysica Acta*, *1854*, 1737–1745.
- Westheimer, F. H. (1968). Pseudo-rotation in the hydrolysis of phosphate esters. *Accounts of Chemical Research*, *1*, 70–78.
- Wilcox, J. L., Ahluwalia, A. K., & Bevilacqua, P. C. (2011). Charged nucleobases and their potential for RNA catalysis. *Accounts of Chemical Research*, *44*, 1270–1279.
- Wong, K. Y., Gu, H., Zhang, S., Piccirilli, J. A., Harris, M. E., & York, D. M. (2012). Characterization of the reaction path and transition states for RNA transphosphorylation models from theory and experiment. *Angewandte Chemie (International Ed. in English)*, *51*(3), 647–651.
- Wong, K. Y., Xu, Y., & Xu, L. (2015). Review of computer simulations of isotope effects on biochemical reactions: From the Bigeleisen equation to Feynman's path integral. *Biochimica et Biophysica Acta*, *1854*, 1782–1794.